Cell Adhesion

International Edition: DOI: 10.1002/anie.201911383
German Edition: DOI: 10.1002/ange.201911383

Phosphorylation Reduces the Mechanical Stability of the α-Catenin/β-Catenin Complex

*Shimin Le[+], Miao Yu[+], and Jie Yan**

Abstract: *The α-catenin/β-catenin complex serves as a critical molecular interface involved in cadherin–catenin-based mechanosensing at the cell–cell adherence junction that plays a critical role in tissue integrity, repair, and embryonic development. This complex is subject to tensile forces due to internal actomyosin contractility and external mechanical micro-environmental perturbation. However, the mechanical stability of this complex has yet to be quantified. Here, we directly quantified the mechanical stability of the α-catenin/β-catenin complex and showed that it has enough mechanical stability to survive for tens to hundreds of seconds within physiological level of forces up to 10 pN. Phosphorylation or phosphotyrosine-mimetic mutations (Y142E or/and T120E) on β-catenin shorten the mechanical lifetime of the complex by tens of fold over the same force range. These results provide insights into the regulation of the α-catenin/β-catenin complex by phosphorylation.*

Introduction

In multicellular organisms, stable adhesions formed between neighboring cells underlie tissue morphogenesis and homeostasis. Cell adhesions also play crucial roles during embryonic development.[1] Defects in the adhesions would lead to tumorigenesis and metastasis for adult organisms.[2] Adherens junctions (AJ), a crucial mediator of intercellular adhesions, contain a highly conserved cadherin–catenin complex, in which the extracellular region of classical cadherins mediates the physical interaction between cells.[3] The cytoplasmic domain of cadherins binds to β-catenin, which in turn binds to α-catenin.[3] The cadherin/β-catenin/α-catenin complex binds to an actin filament in a force-dependent manner,[4] thereby physically linking the cadherin–catenin complex to the actin cytoskeleton. In tissue, the cadherin–catenin physical linkage is subject to tensile forces due to internal actomyosin contractility and perturbation of the external mechanical micro-environment.[5] The mechanical stabilities of these critical interprotein interfaces are critical for the formation and regulation of the stable adhesions.

Previous biochemical and structural studies have demonstrated that the α-catenin/β-catenin complex forms through the N-terminal N1 domain of α-catenin (αN1) and the N-terminal tail of β-catenin (βNt).[6] Furthermore, cell biology studies have shown that phosphorylation of a tyrosine residue (Y142) and/or a threonine residue (T120) on βNt leads to disrupted AJs, which has been hypothesized to be caused by phosphorylation-induced destabilization of the α-catenin/β-catenin complex.[7] However, due to various technological difficulties, quantification of the mechanical stability of interprotein interfaces over a physiological force range has been challenging. As a result, the mechanical lifetime of the critical α-catenin/β-catenin complex has not been quantified, and thus the hypothesis of phosphorylation-induced destabilization of the complex under force has not been experimentally tested.

In this work, utilizing a single-molecule construct design, we directly quantified the mechanical stability of the α-catenin/β-catenin complex over the physiological force range (typically a few pN[8]). We found that the complex has sufficient mechanical stability to survive for tens to hundreds of seconds within a physiological level force range up to 10 pN. Importantly, a phosphotyrosine-mimetic mutation (Y142E) on β-catenin shortens the mechanical lifetime of the complex by 10–100 fold over the same force range. Furthermore, phosphomimetic mutation of both tyrosine (Y142E) and threonine (T120E) on β-catenin causes a further 10–100 fold decrease in the mechanical stability of the complex. Together, these results provide important insights into our understanding of the mechanical-chemical regulation of cadherin–catenin-based cell–cell adhesions.

Results and Discussion

Single-Molecule Construct Design for the α-Catenin/β-Catenin Complex.

Utilizing a single-molecule construct assay for interprotein interactions, we designed a single-molecule construct for direct and efficient quantification of the mechanical stability of the α-catenin/β-catenin complex and the effects of phosphorylation. In the single-molecule construct, the αN12 (the N1 and N2 domains of α-catenin) and βNt[6] are linked

[*] Dr. S. Le,[+] Dr. M. Yu,[+] Prof. Dr. J. Yan
Mechanobiology Institute, National University of Singapore
Singapore 117411 (Singapore)
and
Department of Physics, National University of Singapore
Singapore 117542 (Singapore)
E-mail: phyyj@nus.edu.sg
[+] These authors contributed equally to this work.
Supporting information and the ORCID identification number(s) for the author(s) of this article can be found under: https://doi.org/10.1002/anie.201911383.

through a long, flexible, unstructured polypeptide chain[9] (196 amino acids), and are spanned between four titin Ig 27th domain (I27).[10] The N- and C- termini of the construct contain a biotinylated avi-tag and a spy-tag, respectively, for specific tethering[11] (Figure 1). The four repeats of the well-characterized I27 domain (two repeats at each end) of the essential component act as a molecular spacer. The I27 domain is highly mechanically stable and it unfolds with an unfolding rate of approximately $10^{-3}\,s^{-1}$ over the force range of 2–20 pN.[10] Furthermore, there is a 572-bp DNA handle added between the single-molecule construct and the super-paramagnetic bead as additional spacer to avoid non-specific interaction between the bead and surface. The force on the molecule can be well controlled, and the corresponding force-dependent bead height can be recorded in real time by a magnetic tweezers setup.[12] More details of the single-molecule construct, the surface tethering, and the magnetic tweezers experiments can be found in Texts S1 and S2 in the Supporting Information.

At sufficiently low forces, the αN12 and βNt on the single-molecule construct form a complex, looping the long flexible linker. When the force is increased, the αN12/βNt complex can be ruptured, releasing the looped long flexible linker, resulting in a large stepwise extension jump, which in turn leads to a corresponding stepwise bead-height jump. When the force is reduced, the ruptured complex can be re-formed at low forces. Thereby, the same single-molecule construct can be reused for multiple force-increase and force-decrease cycles (Figure 1). The design converts an intermolecular interaction into an intramolecular interaction, which results in a highly efficient direct quantification of the mechanical lifetime of the complex.

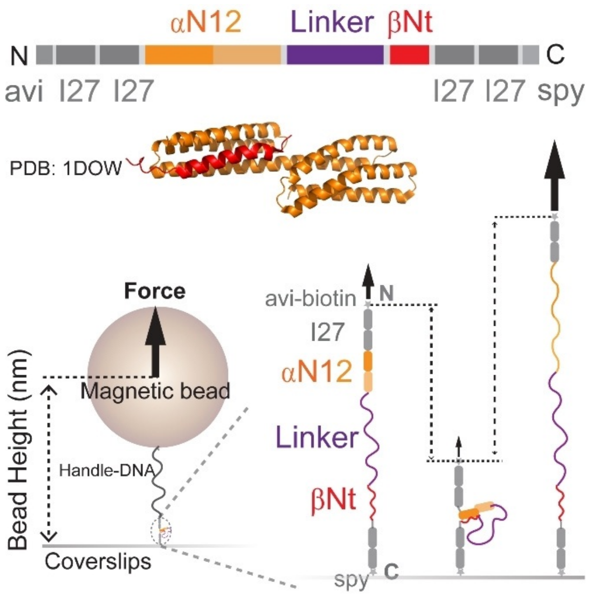

Figure 1. Single-molecule construct design for αN12/βNt complex. Top: design of the single-molecule construct of the αN12/βNt complex. From the N-to-C terminus: an avi-tag, two repeats of the 27th titin immunoglobulin domain (I27), the N1 and N2 domains from α-catenin (αN12), a long flexible unstructured peptide linker (L), the tail motif of β-catenin (βNt), and two repeats of the 27th titin immunoglobulin domain (I27), and finally a spy-tag. The avi-tag and spy-tag are used for specific tethering. The I27 domains are used as a molecular spacer. Middle: Structure of a chimera of α- and β-catenin (PDB: 1DOW).[6] Orange = αN12; Red = βNt. Bottom: in single-molecule stretching experiments, the construct is specifically tethered between a paramagnetic bead (through a 572-bp DNA handle) and a coverslip surface. At low forces, the αN12 and βNt on the construct can form a complex. When the force is increased, the αN12/βNt complex ruptures and αN12 unfolds, leading to bead-height jumps. More details of the construct design can be found in Text S1 in the Supporting Information.

Mechanical Stability of the α-Catenin/β-Catenin Complex.

The top panel of Figure 2a shows the typical force–bead-height curves of the αN12/βNt construct with a force-increase loading rate of $1\,pN\,s^{-1}$ in 1x PBS buffered solution. During a force-increase scan, a large stepwise bead-height jump of 73.5 ± 5.9 nm was observed at 11 ± 1.2 pN (mean ± standard deviation, Figure 2a), corresponding to the rupture of the αN12/βNt complex with concurrent unfolding of one of the αN12 domains (Supporting Information, Figures S1 and S2 and Texts S2 and S3). After the rupture of the complex, the other domain of αN12 unfolded at a force of 13.2 ± 1.7 pN, indicated by the second stepwise bead-height jump of 24.8 ± 3.4 nm (Figure 2a). After rupturing the complex and unfolding both domains in αN12, the force on the construct was then decreased to approximately 1 pN for approximately 60 s to enable the refolding of the domains and formation of the complex. After forming the complex at low force, the construct went through subsequent force-increase scans.

By performing multiple ($N > 100$) force-scan cycles with multiple (more than 5) independent constructs at three loading rates of $0.2\,pN\,s^{-1}$ (orange), $1\,pN\,s^{-1}$ (red), and $5\,pN\,s^{-1}$ (blue), we obtained a two-dimensional (2D) graph of force-dependent transition step sizes of the αN12/βNt construct (middle panel, Figure 2a). The colored circles in the panel are force-dependent step size of the rupture events, and the colored triangles are the second unfolding events of one of the domains in αN12. The dashed curves are the theoretical estimations of the force-dependent step size of several different transitions: 1) the αN12/βNt complex ruptures with concurrent unfolding of both domains in αN12 (top dashed line); 2) the αN12/βNt complex ruptures with concurrent unfolding of one of the domains in αN12 (middle dashed line); 3) Unfolding of one the domains in αN12 (αN2 assumed, bottom dashed line). Details of the theoretical calculation can be found in Text S2 in the Supporting Information. Clearly, the force-dependent step sizes of complex-rupture and domain-unfolding transitions are overall consistent with these theoretical estimations.

We then analyzed the distributions of the rupture forces of the αN12/βNt complex (bottom panel, Figure 2a) at the three force-loading rates, which show peak forces of 8.5 ± 1.2 pN, 11 ± 1.2 pN, and 12 ± 1.8 pN, respectively. The normalized rupture-force histogram at each loading rate can be fitted with the probability of the rupture forces, $\rho_r\,(F) = \frac{k(F)}{r} e^{-\int_{F_0}^{F} k(f')\frac{df'}{r}}$, where r is a given force-loading rate, F_0 is the initial force, F is

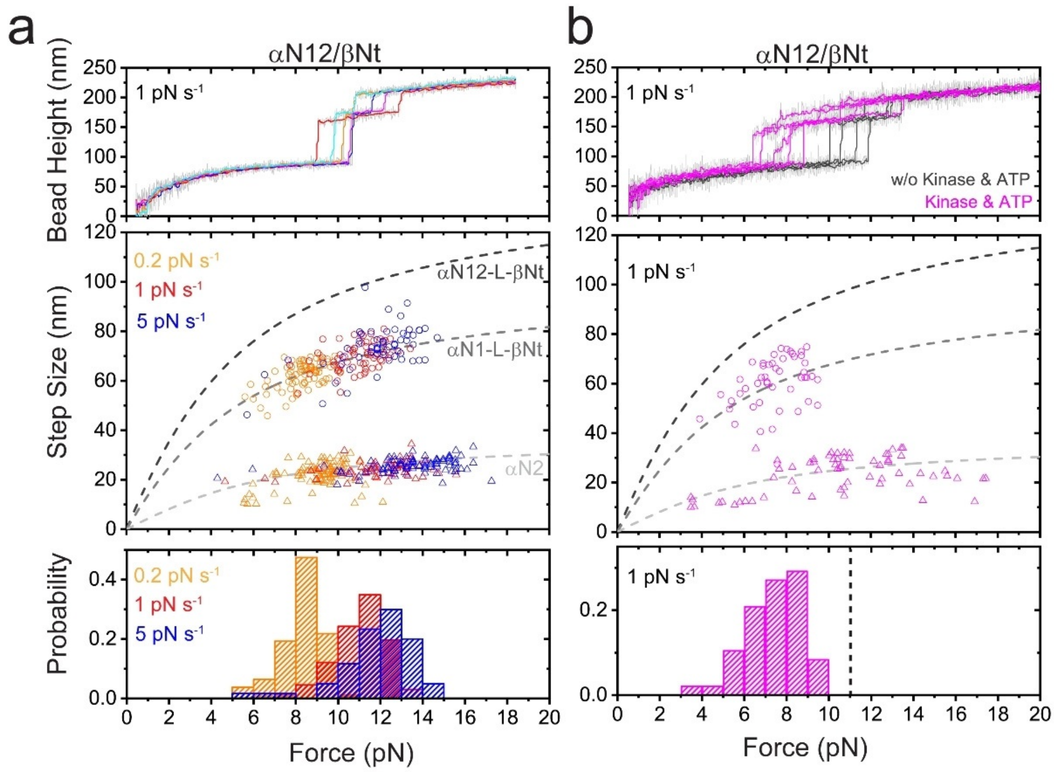

Figure 2. Typical force-induced rupture curves of the αN12/βNt complex with/without kinase phosphorylation. a) Top panel: typical force-height curves of the αN12/βNt complex at a loading rate of 1 pN s^{-1} in 1x PBS solution. Five consecutive force-increase scan curves are indicated by colored lines, which are obtained by 10-point FFT smoothing the raw data in gray. Middle panel: 2D graph of the force-dependent steps sizes of the transitions observed during the force-increase scans at a loading rate of 0.2 pN s^{-1} (orange), 1 pN s^{-1} (red), or 5 pN s^{-1} (blue). The first larger step of rupture transition in each scan is indicated by a colored hollow circle, while the second smaller step of domain unfolding is indicated by a colored hollow triangle. The dashed curves in the panel are theoretical estimations of the force-dependent step sizes for three potential transitions: 1) αN12-L-βNt (top): αN12/βNt complex ruptures with concurrent αN12 unfolding; 2) αN1-L-βNt (middle): αN12/βNt complex ruptures with concurrent αN1 unfolding; 3) αN2 (bottom): unfolding of αN2 at the second step. More details of the theoretical estimations can be found in Text S2 in the Supporting Information. Bottom panel: The normalized histograms of rupture-force distributions at 0.2 pN s^{-1} (orange), 1 pN s^{-1} (red), or 5 pN s^{-1} (blue). The histograms are plotted based on $N=118$, $N=107$, and $N=100$ data points, respectively. b) Top: typical force–height curves of the αN12/βNt complex before (dark gray) and after (magenta) adding kinase and ATP at a loading rate of 1 pN s^{-1} in the standard kinase buffer solution. Middle: 2D graph of the force-dependent step sizes of the transitions observed during the force-increase scans at a loading rate of 1 pN s^{-1} (magenta) after incubation with kinase and ATP. The dashed curves in the panel are the theoretical estimations of the force-dependent step sizes for three potential transitions. Bottom: The normalized histograms of rupture-forces distributions ($N=42$) at 1 pN s^{-1} (magenta) after incubation with kinase and ATP, obtained from 3 out of 11 tested molecules. The dashed vertical line indicates the mean value of the rupture force of the wild-type complex at 1 pN s^{-1} loading rate.

the force at which a transition occurs, and $k(F)$ is the force-dependent rupture rate. $k(F)$ can be described by Bell's model $k_u^{\mathrm{Bell}}(F) = k_u^0 \exp(\beta F \Delta)$, where $\beta = \frac{1}{K_B T}$, Δ is the transition distance of the complex rupture, and k_u^0 is the extrapolated zero-force rupture rate (Supporting Information, Texts S4 and S5). The best fitting of the histograms determines the k_u^0 and Δ for the rupture of the complex to be $1.8 \pm 3.1 \times 10^{-4}\ s^{-1}$ and 4.1 ± 0.8 nm, respectively.

Tyrosine Phosphorylation Decreases the Mechanical Stability of α-Catenin/β-Catenin Complex.

Phosphorylation of the critical residues (such as tyrosine 142, Y142) on βNt leads to disrupted AJs, which has been hypothesized to be resulted from phosphorylation-induced destabilization of the α-catenin/β-catenin complex under force.[7] To test this hypothesis, we first stretched the αN12/βNt construct in the standard tyrosine kinase buffer solution of 20 mM HEPES pH 7.5, 100 mM NaCl, 10 mM $MgCl_2$, 3 mM $MnCl_2$, 1.5 mM Na_3VO_4, 1% BSA, 2 mM DTT, 10 mM sodium L-ascorbate at 21 ± 1 °C. In the absence of tyrosine kinase, in all 11 molecules tested, the rupture forces of the αN12/βNt molecules were about 10–12 pN at the loading rate of 1 pN s^{-1} (dark gray curves in Figure 2b, top panel), similar with that obtained in 1x PBS solution. In contrast, after incubation with 10 nM active FAK (focal adhesion kinase that targets tyrosines) and 1 mM ATP, three of 11 molecules ruptured at decreased forces of 4–8 pN at the same loading rate (magenta, Figure 2b, bottom panel). The corresponding 2D graph (Figure 2b, middle panel) of force-dependent step size of the rupture transition suggests the rupture of the complex is still concurrent with the unfolding of one of the domains of αN12. The absence of stability decrease with the other molecules could be explained by unsuccessful phosphorylation of the residue over the incubation time.

Phosphomimetic Mutations Decrease the Mechanical Stability of the α-Catenin/β-Catenin Complex.

The decreased mechanical stability of some of the tested αN12/βNt constructs in the presence of FAK suggests that the Y142 residue of βNt in these constructs was successfully phosphorylated and that the single-residue phosphorylation leads to the decreased mechanical stability of the complex. To further test this, we investigated the mechanical stability of the complex using a new construct αN12/βNt^{Y142E} with a single-residue phosphotyrosine-mimetic mutation in βNt (Y142E), which ensures that 100% of the molecules possess a phosphorylation mimic.

The top panel of Figure 3a shows typical force–bead-height curves of the αN12/βNt^{Y142E} construct at a loading rate of 1 pN s^{-1} in 1x PBS buffered solution. The middle panel shows the resulting 2D graph of the force-dependent step size of the complex rupture and domain-unfolding transitions obtained at loading rates of 1 pN s^{-1} (red) and 5 pN s^{-1} (blue), and the bottom panel shows the resulting normalized rupture-force histograms of the αN12/βNt^{Y142E} construct at the corresponding loading rates. Indeed, the Y142E mutation of the βNt leads to decreased mechanical stability of the complex compared to the αN12/βNt complex, resulting in much lower peak rupture force of the complex at 6.4 ± 1.5 pN and 7.6 ± 1.6 pN at loading rates of 1 pN s^{-1} and 5 pN s^{-1}, respectively, for all the 9 molecules tested. The distribution of the rupture force of the αN12/βNt^{Y142E} complex is in a similar range of that obtained for αN12/βNt in presence of FAK.

Besides the Y142 residue, there is another phosphorylation residue within βNt, which is the threonine residue, T120. Hence, we further asked whether the phosphorylation of both of these critical residues would further affect the mechanical stability of the αN12/βNt complex. To test this, we prepared

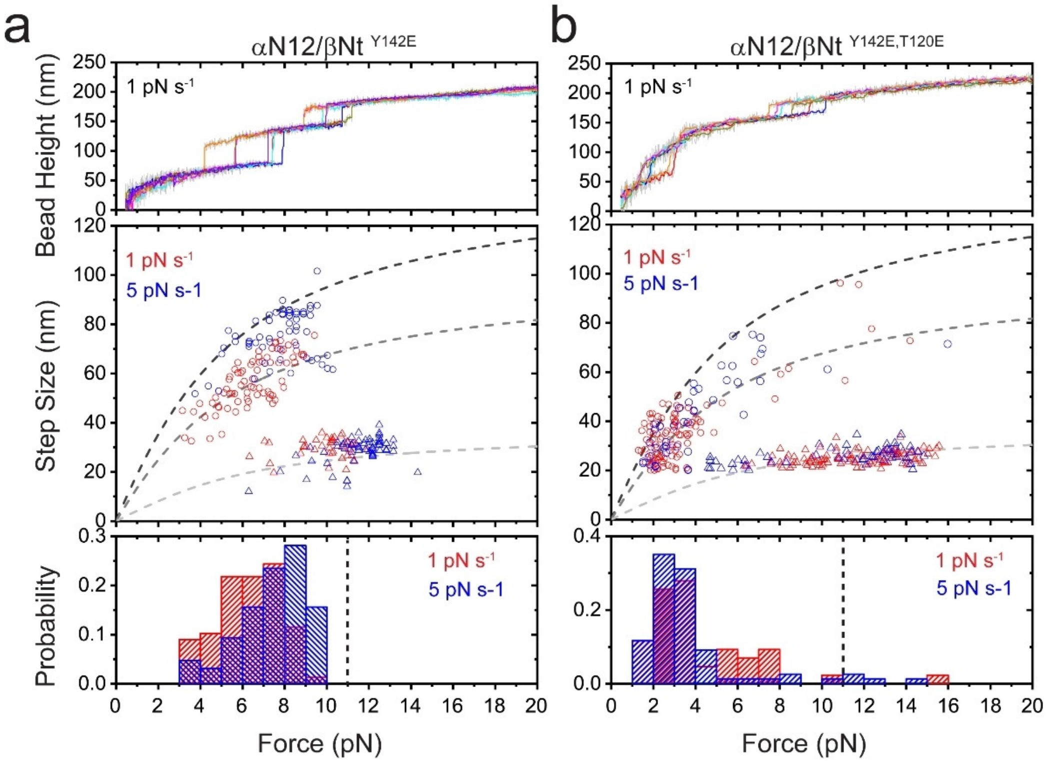

Figure 3. Typical force-induced rupture curves of the αN12/βNt complex with Y142E mutation or Y142E and T120E mutations on βNt. a) Top: typical force–height curves of the αN12/βNt^{Y142E} complex at a loading rate of 1 pN s^{-1} in 1x PBS solution. Five consecutive force-increase scan curves are indicated by colored lines, which are obtained by 10-point FFT smoothing the raw data in gray. Middle: 2D graph of the force-dependent steps sizes of the transitions observed during the force-increase scans at a loading rate of 1 pN s^{-1} (red) or 5 pN s^{-1} (blue). The first larger step of rupture transition in each scan is indicated by a colored hollow circle, while the second smaller step of domain unfolding is indicated by a colored hollow triangle. Bottom: The normalized histograms of rupture-force distributions at 1 pN s^{-1} (red) or 5 pN s^{-1} (blue). The histograms are plotted based on $N = 116$ and $N = 102$ data points, respectively, obtained from 9 molecules. b) Top: typical force–height curves of the αN12/βNt^{Y142E,T120E} complex at a loading rate of 1 pN s^{-1} in 1x PBS solution. Five consecutive force-increase scan curves are indicated by colored lines, which are obtained by 10-point FFT smoothing the raw data in gray. Middle: 2D graph of the force-dependent steps sizes of the transitions observed during the force-increase scans at a loading rate of 1 pN s^{-1} (red) or 5 pN s^{-1} (blue). The first larger step of rupture transition in each scan is indicated by a colored hollow circle, while the second smaller step of domain unfolding is indicated by a colored hollow triangle. The dashed curves in the panel are the theoretical estimations of the force-dependent step sizes for three potential transitions. Bottom: The normalized histograms of rupture-force distributions at 1 pN s^{-1} (red) or 5 pN s^{-1} (blue). The histograms are plotted based on $N = 110$ and $N = 63$ data points, respectively, obtained from 5 molecules. The dashed vertical line indicates the mean value of the rupture force of the wild-type complex at 1 pN s^{-1} loading rate. More details of the theoretical estimations can be found in Texts S2 and S3 in the Supporting Information.

another phosphomimetic mutant, αN12/βNt^{Y142E,T120E}, with both Y142E and T120E mutations, and performed similar force-induced rupture experiments. The top panel of Figure 3b shows the typical force–bead-height curves of the αN12/βNt^{Y142E,T120E} construct at a force-loading rate of $1\ pN\,s^{-1}$. Clearly, the rupture forces (the first stepwise bead-height jumps in the curves) of the αN12/βNt^{Y142E,T120E} complex further decreased to below 4 pN. We plotted the 2D force-dependent step sizes of the transitions and the normalized rupture-force distributions of the αN12/βNt^{Y142E,T120E} complex at $1\ pN\,s^{-1}$ (red) and $5\ pN\,s^{-1}$ (blue) as the middle panel and bottom panel of Figure 3b, respectively. While a small fraction of the rupture events occurs at higher forces (greater than 6 pN), the majority of the rupture forces for the αN12/βNt^{Y142E,T120E} complex were about 2–4 pN for all 5 molecules tested. Together, these results suggest that the double phosphomimetic mutant of the β-catenin tail causes further decrease in the mechanical stability of the α-catenin/β-catenin complex.

Direct Quantification of the Force-Dependent Lifetime of the αN12/βNt Complex.

While the above rupture-force analysis has clearly revealed that the phosphomimetic Y142E and/or T120E mutations result in a decrease in the mechanical stability of the αN12/βNt complex, a more direct view of the mechanical stability is the lifetime of the complex at different constant forces. To provide this information, we implemented a force-clamp-cycle assay: 1) the αN12/βNt construct (or the mutant constructs) was held at less than 1 pN for 30 s to allow formation of the complex; 2) the force was then jumped to a rupture force in the range of 3–15 pN, clamped, and the dwell time was recorded (i.e., lifetime of the complex) until complex rupture was observed; 3) the force was then jumped to less than 1 pN and held there for approximately 30 s to allow the reformation of the complex for the subsequent force-clamp cycle (Figure 4a, representative lifetime measurement at approximately 9.0 pN). For the αN12/βNt construct or the αN12/βNt^{Y142E} construct, the force-clamp procedure was repeated for multiple times (more than 20) on multiple (more than 5) independent constructs at each rupture force in the range of 3–15 pN. For the mechanically weakest αN12/βNt^{Y142E,T120E} construct, we held the construct at constant forces in the range of approximately 1–3 pN and recorded multiple (more than 20) rupture/re-pairing transition dynamics during the constant forces clamping. The average force-dependent lifetime of the complex was obtained by averaging the pool of the dwell times at each force.

Figure 4b shows the resulting average force-dependent lifetime of the αN12/βNt complex (red), the αN12/βNt^{Y142E} complex (magenta), and the αN12/βNt^{Y142E,T120E} complex (blue). Clearly, the wild-type αN12/βNt complex can last several seconds to tens of seconds at forces of 6–10 pN, and can withstand hundreds of seconds at forces below 5 pN. In sharp contrast, the phosphomimetic αN12/βNt^{Y142E} complex has a greatly reduced mechanical stability: the single Y142E mutation results in a several tens of fold decrease in lifetime compared to that of wild-type αN12/βNt complex over the physiological force range. Furthermore, the double mutation of Y142E and T120E leads to a further several tens of fold decrease in lifetime compared to the single mutation.

Figure 5 shows the time-evolution of the dynamics of the constructs at near equilibrium forces (≈ 1.5–2 pN), which also clearly demonstrates the drastic de-stabilization effects on the

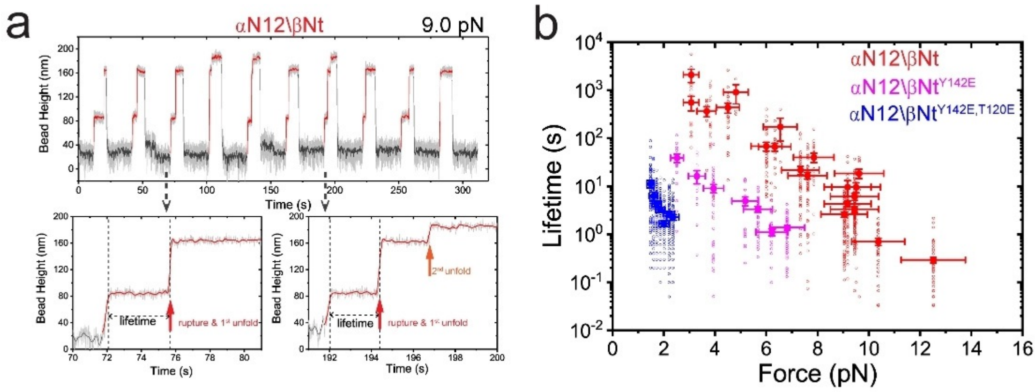

Figure 4. The mechanical lifetime of the αN12/βNt complex with or without phosphomimetic mutations. a) Typical force-jump measurement of the mechanical lifetime of the αN12/βNt complex. The αN12/βNt construct was held at low force of approximately 0.5 pN for approximately 30 s (dark gray lines) to allow formation of αN12/βNt complex, then jumped to a higher rupture-force (for example, approximately 9.0 pN, red lines in the example) until the complex rupture was observed, indicated by the large bead-height jump. The top panel shows examples of multiple force-jump cycles; the bottom panels show two zoomed-in force-jump cycles, where the lifetime of the complex (i.e., the dwell time of the complex before rupture at the force) was indicated by dashed lines. The red arrows indicate the bead-height change induced by the structural transitions (rupturing or unfolding) of the construct. The occasional second bead-height jump of approximately 25 nm is the unfolding of one of the αN domains, presumably the αN2 domain. b) The force-dependent lifetime of the αN12/βNt complex with or without phosphomimetic mutations. The red data are from the wild-type complex, the magenta data are from the complex with the Y142E mutation, and the blue data are from the complex with both Y142E and T120E mutations. The solid symbols are the mean value, while the hollow symbols are the individual experimentally measured lifetimes. The Y-error bar is the standard error of the mean value. The X-error bar represents 10% error of the force measurement. The fittings of the corresponding force-dependent rupture rates of these three complexes are provided in Figure S3 in the Supporting Information.

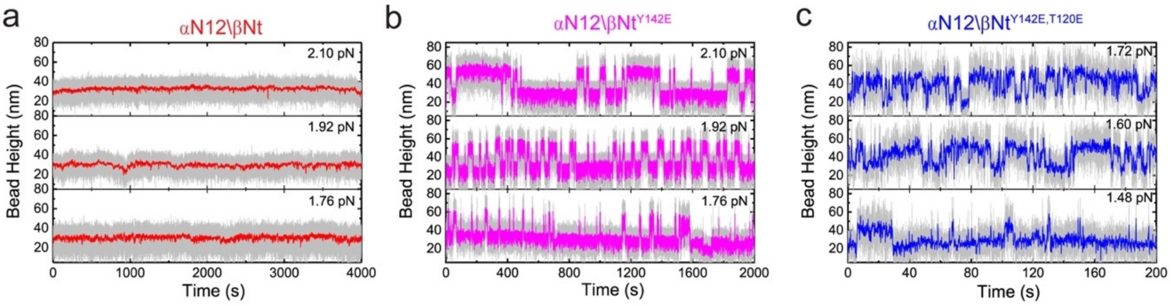

Figure 5. The dynamics of the αN12/βNt complex with or without phosphomimetic mutations. a–c) The time–bead-height curves of the αN12/βNt complex at a low force range of approximately 1.5–2 pN for the wild-type βNt (a), Y142E mutation of βNt (b), and the Y142E and T120E mutation of βNt (c).

mechanical stability of the αN12/βNt complex by the Y142E or/and T120E mutations. For the wild-type αN12/βNt construct, it remains paired over 4000 seconds at the force range (Figure 5a), while the αN12/βNt^{Y142E} is much less stable, with its lifetime reduced to ≈tens of seconds at ≈1.7 pN (Figure 5b). The αN12/βNt^{Y142E,T120E} is even less stable, with the lifetime further decreased to several seconds at the same force of ≈1.7 pN (Figure 5c).

Conclusion

In summary, we directly quantified the mechanical stabilities of the interfaces of α-catenin/β-catenin complex, and the effects of tyrosine-phosphorylation or phosphomimetic mutations (Y142E, T120E on β-catenin) on the mechanical stability of the complex. The lifetime of tens to hundreds of seconds of the α-catenin/β-catenin complex in the physiological force range demonstrates that this mechanical interface can maintain a stable mechanotransduction pathway for cell–cell adhesions. Further, the approximately 10–1000 fold decreased lifetime of the phosphomimetic mutants of the complex provides a direct quantitative molecular mechanism of the phosphorylation-induced disruption of AJs that has been observed in vivo.[7] Single-molecule manipulation technologies are powerful tools to quantify the mechanical stability of protein–protein interactions,[13] the single-molecule construct assay described in this study further facilitates single-molecule technologies for efficient direct quantification of mechanical stabilities of protein–protein interfaces and the effects of biological or chemical modifications on the interfaces.

Acknowledgements

We thank Ms Hongying Chen (protein expression facility, Mechanobiology Institute) for her help in protein purification. The research is funded by the National Research Foundation, Prime Minister's Office, Singapore, under its NRF Investigatorship Programme (NRF Investigatorship Award No. NRF-NRFI2016-03 to J.Y.), the Ministry of Education under the Research Centres of Excellence programme (to J.Y., in part), and Singapore Ministry of Education Academic Research Fund Tier 3 (MOE2016-T3-1–002 to J.Y., in part).

Conflict of interest

The authors declare no conflict of interest.

Keywords: α-catenin · β-catenin · force · mechanotransduction · phosphorylation

How to cite: *Angew. Chem. Int. Ed.* **2019**, *58*, 18663–18669
Angew. Chem. **2019**, *131*, 18836–18842

[1] H. Haegel, L. Larue, M. Ohsugi, L. Fedorov, K. Herrenknecht, R. Kemler, *Development* **1995**, *121*, 3529–3537.
[2] a) E. Farahani, H. K. Patra, J. R. Jangamreddy, I. Rashedi, M. Kawalec, R. K. Rao Pariti, P. Batakis, E. Wiechec, *Carcinogenesis* **2014**, *35*, 747–759; b) T. Takayama, H. Shiozaki, S. Shibamoto, H. Oka, Y. Kimura, S. Tamura, M. Inoue, T. Monden, F. Ito, M. Monden, *Am. J. Pathol.* **1996**, *148*, 39–46; c) T. Utsunomiya, Y. Doki, H. Takemoto, H. Shiozaki, M. Yano, M. Inoue, T. Yasuda, Y. Fujiwara, M. Monden, *Gastric Cancer* **2000**, *3*, 193–201.
[3] S. Yamada, S. Pokutta, F. Drees, W. I. Weis, W. J. Nelson, *Cell* **2005**, *123*, 889–901.
[4] C. D. Buckley, J. Tan, K. L. Anderson, D. Hanein, N. Volkmann, W. I. Weis, W. J. Nelson, A. R. Dunn, *Science* **2014**, *346*, 1254211.
[5] a) G. Charras, A. S. Yap, *Curr. Biol.* **2018**, *28*, R445–R457; b) W. J. Nelson, *Biochem. Soc. Trans.* **2008**, *36*, 149–155.
[6] S. Pokutta, W. I. Weis, *Mol. Cell* **2000**, *5*, 533–543.
[7] a) M. D. David, A. Yeramian, M. Dunach, M. Llovera, C. Canti, A. G. de Herreros, J. X. Comella, J. Herreros, *J. Cell Sci.* **2008**, *121*, 2718–2730; b) F. H. Brembeck, T. Schwarz-Romond, J. Bakkers, S. Wilhelm, M. Hammerschmidt, W. Birchmeier, *Genes Dev.* **2004**, *18*, 2225–2230; c) J. Tominaga, Y. Fukunaga, E. Abelardo, A. Nagafuchi, *Genes Cells* **2008**, *13*, 67–77; d) C. Du, M. Jaggi, C. Zhang, K. C. Balaji, *Cancer Res.* **2009**, *69*, 1117–1124.
[8] N. Borghi, M. Sorokina, O. G. Shcherbakova, W. I. Weis, B. L. Pruitt, W. J. Nelson, A. R. Dunn, *Proc. Natl. Acad. Sci. USA* **2012**, *109*, 12568–12573.
[9] M. Yu, S. Le, A. K. Efremov, X. Zeng, A. Bershadsky, J. Yan, *Nano Lett.* **2018**, *18*, 5239–5247.

[10] G. Yuan, S. Le, M. Yao, H. Qian, X. Zhou, J. Yan, H. Chen, *Angew. Chem. Int. Ed.* **2017**, *56*, 5490–5493; *Angew. Chem.* **2017**, *129*, 5582–5585.

[11] a) S. Le, X. Hu, M. Yao, H. Chen, M. Yu, X. Xu, N. Nakazawa, F. M. Margadant, M. P. Sheetz, J. Yan, *Cell Rep.* **2017**, *21*, 2714–2723; b) B. Zakeri, J. O. Fierer, E. Celik, E. C. Chittock, U. Schwarz-Linek, V. T. Moy, M. Howarth, *Proc. Natl. Acad. Sci. USA* **2012**, *109*, E690–697.

[12] a) H. Chen, H. Fu, X. Zhu, P. Cong, F. Nakamura, J. Yan, *Biophys. J.* **2011**, *100*, 517–523; b) S. Le, R. Liu, C. T. Lim, J. Yan, *Methods* **2016**, *94*, 13–18; c) S. Le, M. Yao, J. Chen, A. K. Efremov, S. Azimi, J. Yan, *Nucleic Acids Res.* **2015**, *43*, e113.

[13] a) C. Schoeler, K. H. Malinowska, R. C. Bernardi, L. F. Milles, M. A. Jobst, E. Durner, W. Ott, D. B. Fried, E. A. Bayer, K. Schulten, H. E. Gaub, M. A. Nash, *Nat. Commun.* **2014**, *5*, 5635; b) K. Halvorsen, D. Schaak, W. P. Wong, *Nanotechnology* **2011**, *22*, 494005; c) M. Yu, S. Le, Y. C. Ammon, B. T. Goult, A. Akhmanova, J. Yan, *Nano Lett.* **2019**, *19*, 5982–5990.

Manuscript received: September 6, 2019
Version of record online: November 4, 2019

